Optoelectronic Materials ISSN 2377-4738 *Optoelectron Mater.* ***1*** *(2016) 57–62*

Vertically aligned ZnO nanotubes for filter-free photocatalytic degradation of methyl orange in water

Qiao-xia Yin, Long Yang, Bao-gai Zhai, Lei Cai, Yuan Ming Huang*

School of Mathematics and Physics, Changzhou University, Jiangsu 213164, China

(*Received 27 October 2016; accepted 16 December 2016*)

Vertically aligned ZnO nanotubes with the average length of 1 μm, outer diameter of around 500 nm and wall thickness of about 30 nm were grown on glass substrates by hydrothermal growth and subsequent selective etching of ZnO nanorods in solutions. The crystal structures and the kinetics of photocatalytic activity of the ZnO nanotubes were investigated by means of the scanning electron microscopy, X-ray diffractometry, photoluminescence spectroscopy and UV-Vis spectroscopy. Under the illumination of 100 W high-pressure mercury lamp, the chemical kinetics of photocatalytic degradation is presented, and the first-order photocatalytic constant of the vertically ZnO nanotubes has been found to increase linearly from 2.6×10^{-3} to 2.3×10^{-2} min^{-1} as the catalyst loading increases from 75 to 900 mg/L. With the advantage of excellent recyclability, ZnO nanotubes in the form of immobilized films can find large-scale applications as filter-free and cost-effective photocatalysts for water treatment.

Keywords: ZnO nanotube; Photocatalysis; Hydrothermal growth; First-order photocatalytic constant; Photoluminescence

1. Introduction

With the merits of high surface-to-volume ratio and exceptional optical properties, a variety of ZnO nanostructures (nanoparticles [1], nanorods [2,3], nanotubes [4,5], nanospheres [6,7], nanoleaves [8]) have been intensively studied as photocatalysts to degrade organic contaminants in water. In most of the photocatalytic studies, the photocatalytic activities were evaluated for the ZnO nanostructures in the form of nanoparticles [1,2,6-8]. Although ZnO nanostructures in the form of nanoparticles are very effective photocatalysts, it is found that subsequent removal of the ZnO nanoparticles from purified water can be cumbersome and expensive because filtration is needed in the stage of post-degradation treatment. In order to reduce the operation costs, filter-free ZnO photocatalysts should be developed for photocatalytic degradation of organic contaminants in water.

It is known that immobilized photocatalysts can reduce the cost of filtration and also in some cases increase the efficiency of a photocatalyst. With the advantages of hollow structures to provide large surface area for photocatalytic reactions, vertically aligned ZnO nanotubes in the form of immobilized films can be developed into highly efficient photocatalyst for large-scale and cost-effective water treatment. As documented in the literature, Chu et al. reported that 60 mL of methyl blue (20 mg/L) could be degraded by one piece of ZnO nanotube film under the ultraviolet irradiation from 110 W ultraviolet lamp for 90 min [4]; Xu et al. reported that 20 mL of methyl orange (50 μM) could be decomposed under the ultraviolet irradiation from a 300 W high-pressure Hg lamp for 90 min [5]. It has long been established that: (i) photolysis of organics is often observed when organics are illuminated with ultraviolet and visible light [3,9]; (ii) both the kinetics and the first-order photocatalytic rate constant are the important aspects of photocatalysts [10,11]; and (iii) the photocatalytic activity of ZnO catalysts is generally complicated by numerous factors, among which the morphology [1,2], the specific surface area, and the defect density in the catalysts [2] and the loading of the catalysts are critically important ones [10-13]. However, detailed analysis of the available data reveals that: (i) the photolysis of the organics was not taken into account; (ii) neither the kinetics nor the first-order photocatalytic rate constant of the photocatalytic degradations was determined; and (iii) the effect of catalyst loading on the first-order photocatalytic rate constant was not investigated [4,5]. Therefore, further investigations on the photocatalytic activity of vertically aligned ZnO nanotubes are required. In this paper, we report the study on the photocatalytic activity of vertically aligned ZnO nanotubes immobilized on glass substrates. The kinetics of photocatalytic degradations is determined, and its dependence on catalyst loading is presented.

*Corresponding author. Email: dongshanisland@126.com

2. Materials and characterizations

2.1 Synthesis of vertically aligned ZnO nanotubes

Vertically aligned ZnO nanotubes were synthesized on glass substrates (5 × 2.5 cm2) by hydrothermal growth and subsequent selective etching of ZnO nanorods in solutions. As described in previous work [14-16], vertically ZnO nanorods were grown onto the glass substrate via the hydrothermal route: (i) ZnO seeding solution was prepared at 60°C by dissolving zinc acetate dihydrate (3.3 g) and ethanolamine (1.8 ml) into ethanol (50 ml); (ii) a ZnO seed layer was formed on the glass substrate by dipping the cleaned glass substrate into the ZnO seeding solution for about 1 min and then dried at 300°C for 10 min (3 cycles); (iii) the ZnO seed layer coated glass substrate was put into in a Teflon – lined stainless steel autoclave for reaction at 93°C for 4 h. 40 ml of equal molar aqueous solution of zinc nitrate (0.15 M) and hexamethylene tetramine (0.15 M) was filled in the autoclave. After the hydrothermal growth, the glass substrate was taken out the autoclave, rinsed with deionized water and then dried in the air. The subsequent selective etching of the ZnO nanorods on the glass substrate was performed in ammonium solution (0.5 wt%)

at room temperature by vertical suspension of the ZnO nanorods upside down in the aqueous solution of ammonia (100 ml) for 12 hours. The ZnO nanotubes on one piece of glass substrate was weighted to be 15 mg. Dozens of identical glass substrates were prepared to grow the vertically aligned ZnO nanotubes under the same conditions as described above.

2.2 Structural and optical characterizations

The scanning electron microscope (SEM, JSM-6360LA, Japan) was employed to analyze the morphology of the ZnO nanotubes whilst the X-ray diffractometer (XRD, D/max 2500 PC, Japan) was utilized to analyze the crystal structures of the ZnO nanotubes. A copper target was utilized to generate the X-ray (λ=0.154 nm). The photoluminescence (PL) spectra of the ZnO nanoleaves were recorded with a spectrophotometer (Tianjin Guangdong Ltd., China). The 325-nm laser line from a helium-cadmium laser was utilized as the excitation source for the PL measurement. Details on the instruments and their operating parameters were described elsewhere [14-16].

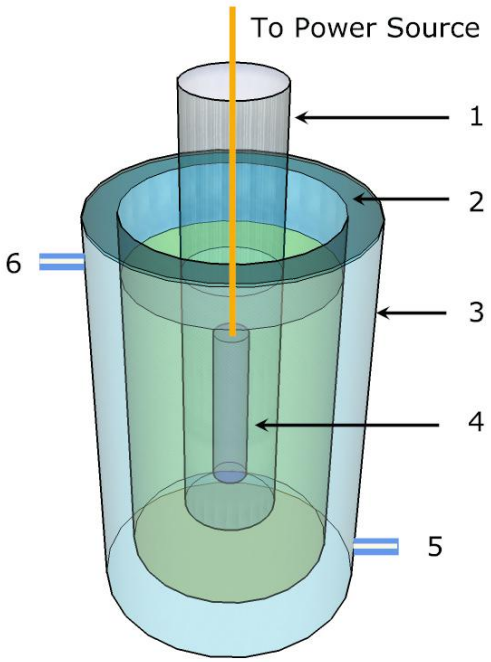

Fig. 1 Schematic illustration of the photocatalytic reactor. 1: an inner cylindrical quartz tube (ϕ55 mm) to house the high-pressure mercury lamp. 2: a middle cylindrical glass tube (ϕ85 mm) to reserve the dye solution. 3: an outer cylindrical glass tube to contain the cooling water. 4: a high ─ pressure mercury lamp. 5: inlet of the cooling water. 6: outlet of the cooling water.

2.3 Specific surface area of ZnO nanotubes

The specific surface area of ZnO nanotubes was measured using a surface area analyzer (Micromeritics ASAP2010C) on the basis of nitrogen absorption at -196 ° C. ZnO nanotubes were scratched off the glass substrates. The samples were degassed under 0.01 mmHg overnight at 150 ° C before nitrogen adsorption. The obtained nitrogen adsorption-desorption isotherms were evaluated with the Brunauer – Emmett – Teller (BET) equation to give the values of their specific surface areas. The BET specific surface area of ZnO nanotubes was derived to be around 29 m^2/g. TiO2 nanoparticles (P25, Degussa) were used as a reference, and the BET specific surface area of P25 was derived to be 50 m^2/g when characterized under identical conditions.

2.4 Evaluation of the photocatalytic activity

The photocatalytic activity of vertically aligned ZnO nanotubes was evaluated by monitoring the degradation of methyl orange in water under the irradiation from a high – pressure mercury lamp. Fig. 1 schematically illustrates the setup of the photocatalytic reactor. As shown in Fig. 1, the reactor consists of a high-pressure mercury lamp, an inner cylindrical quartz tube (ϕ55 mm) to house the mercury lamp, a middle cylindrical glass tube (ϕ85 mm) to contain the methyl orange solution for photocatalytic degradation, and an outer cylindrical glass tube (ϕ135 mm) to reserve the cooling water. In the inner cylindrical quartz tube, the high – pressure mercury lamp was aligned along the central axis of the inner quartz tube. The output power of the high-pressure mercury lamp was 100W, the primary emission lines of the lamp were located at 365.0, 404.7, 435.8 and 546.1 nm. The free space between the inner and the middle tubes was filled with 400 ml of the methyl orange solution (11.25 mg/L). Tape water was running in the space between the middle and the outer tubes to keep the temperature of the methyl orange solution lower than 40 °C. The vertically aligned ZnO nanotubes on a pair of glass substrates were immersed into the methyl orange solution with the ZnO nanotubes facing to the high – pressure mercury lamp. The catalyst loading was 75 mg/L for a pair of glass substrates immobilized with vertically aligned ZnO nanotubes. The solution of methyl orange was magnetically stirred in dark for 30 min to ensure the establishment of an adsorption – desorption equilibrium. After having been exposed to the irradiation for a certain period of time, 5 ml of the suspension was collected for absorbance measurement. The concentration of methyl orange was determined by checking the absorbance using an ultraviolet – visible spectrophotometer (UV2450, Shimazu) [6-8].

3. Results and discussions

3.1 Morphology and crystal structure of ZnO nanotubes

Fig. 2 shows the SEM micrographs of the vertically aligned ZnO nanotubes on glass substrate. It can be seen in Fig. 2 that the ZnO nanotubes are closely packed with their hexagonal side walls discernible clearly. The tube axes of these highly oriented ZnO nanotubes are perpendicular to the glass substrates. On the basis of statistics over a large number of ZnO nanotubes grown on the substrate, the average length, outer diameter, wall thickness and population density of the ZnO nanotubes were derived to be around 1 μm, 500 nm, 35 nm and 7.8 × 108 cm^{-2}, respectively. It is well known that hexagonal ZnO crystal is composed of polar faces (001) and nonpolar faces (110), among which the polar faces (001) have relatively higher surface energy whilst the non-polar faces (110) have lower surface energy. The

surface energy difference between the polar and non-polar surfaces drives the preferential growth of ZnO nanorods along the [001] direction in order to minimize the total surface energy. The mechanisms on the hydrothermal growth of ZnO nanorods were discussed in the literature [17,18]. In the etching process, hydroxyl ion (OH-) and NH^{4+} are present in the ammonia solution. As mentioned above, ZnO is a polar crystal, the polar faces (001) of ZnO nanocrystal are either positively charged or negatively charged. ZnO with positive polar is rich in Zn whereas the negative polar is rich in oxygen. The positively charged ZnO nanorod surfaces (001) attract more polar molecules OH- for subsequent ZnO dissolution. In the same time, the negatively charged ZnO nanorod surfaces (001) will attract more polar molecules NH^{4+} for subsequent ZnO dissolution. So the etching rate of the polar planes (001) is faster than that of the nonpolar lateral planes (110). Consequently, ZnO nanotubes are resulted due to the preferential etching along the c-axis of ZnO nanorods. The mechanisms on the selective etching of the ZnO nanorods were discussed in the literature [19,20].

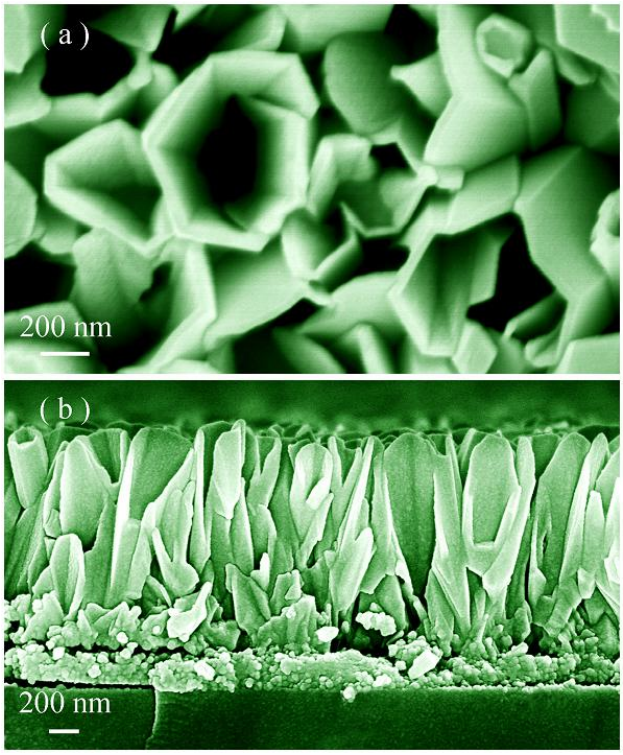

Fig. 2 Top-view (top panel) and cross-sectional (bottom panel) SEM micrographs of the vertically aligned ZnO nanotubes grown on a glass substrate.

To check the phase and purity of ZnO nanotubes, we performed XRD analysis on the vertically aligned ZnO nanotubes. Fig. 3 depicts the XRD spectrum of the vertically aligned ZnO nanotubes. It is important to notice the logarithmic scale of the XRD intensity in order to show the weak peaks clearly. As shown in Fig. 3, the recorded diffraction peaks at 2θ = 31.62, 34.35, 36.22, 47.45, 56.58, 62.84, 67.91 and 72.60° can be assigned to the (100), (002), (101), (102), (110), (103), (112) and (004) planes of wurtzite ZnO, respectively [13-21]. According to the Bragg diffraction equation, the lattice constants a and c of the ZnO nanotubes were derived to be 0.327 and 0.523 nm, respectively, which are in good agreement with the standard lattice constants of wurtzite ZnO. The strongest peak (002) suggests that the ZnO nanotubes are preferentially aligned along the c-axis. The texture coefficients (TCs), which is defined by Eq. (1), can be employed to evaluate the degree of orientation of ZnO nanocrystals

$$TC_{(hkl)} = \frac{I_{(hkl)} / I^{o}_{(hkl)}}{(1/N)\sum I_{(hkl)} / I^{o}_{(hkl)}} \qquad (1)$$

where N is the number of diffraction peaks, $I(hkl)$ is the experimentally measured intensity of the diffraction peak (hkl), $I_0(hkl)$ is the recorded intensity of the (hkl) diffraction peak according to the JCPDS 036-1451 card [22]. According to Eq (1), the TCs for the 8 diffraction peaks were calculated to be 0.43, 6.05, 0.58, 1.00, 0.18, 0.89, 0.22 and 1.65, respectively. The high value of TC(002) indicates that the ZnO nanotubes are well aligned with their tube axes along the (002) orientation.

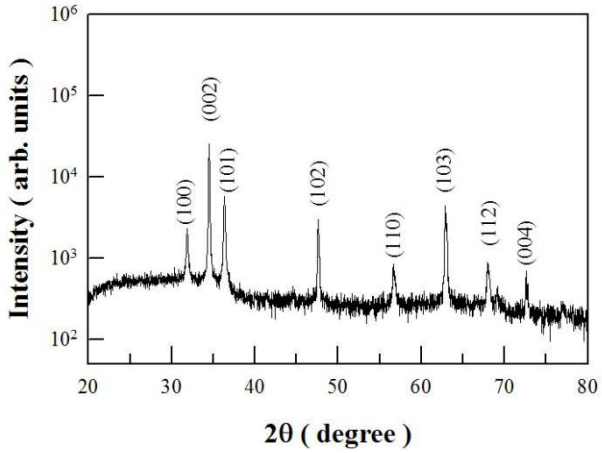

Fig. 3 XRD spectrum of vertically aligned ZnO nanotubes grown on a glass substrate.

3.2 Photoluminescence spectrum of ZnO nanotubes

Fig. 4 illustrates the PL spectrum of the vertically aligned ZnO nanotubes. The hollow circles in Fig. 4 represent the experimental data. As discussed in our previous report [16,23], the PL spectrum in Fig. 4 can be deconvoluted into three Gaussian components, i.e., a near ultraviolet band (shaded in blue) with its peak centered at 380.0 nm, a green (shaded in green) band with its peak centered at 536.7 nm, and a red band (shaded in yellow) with its peak centered at 626.3 nm. The sum of the three Gaussian components is represented by the red solid curve in Fig. 4. It is known that a variety of defects are present in ZnO nanocrystals, among which include oxygen vacancies (V_o), zinc vacancies (V_{Zn}), oxygen atoms at the Zn position in the crystal lattice (O_{Zn}) and donor – acceptor pairs [24]. The ultraviolet PL band at around 380 nm is generally attributed to the band-edge recombination of excitons whilst the green and red PL bands are produced by defects in ZnO nanorods [13-15,21-26]. Therefore, the PL spectrum in Fig. 4 indicates that a lot of defects are present in the vertically aligned ZnO nanotubes. On one hand, if the defects act as

luminescent centers, they are negative to an efficient photocatalyst because they capture photogenerated electrons or holes and then recombine them in the form of emitting photons. On the other hand, it was reported that higher photocatalytic activity can be expected if the defects in ZnO nanotubes act as the active centers of the catalysts by capturing the photogenerated electrons or holes and then decreasing the recombination of the photogenerated carriers [3,5].

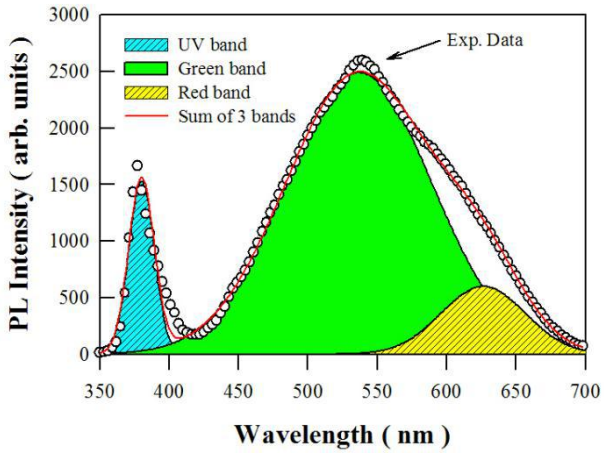

Fig. 4 PL spectrum of vertically aligned ZnO nanotubes and its three Gaussian components.

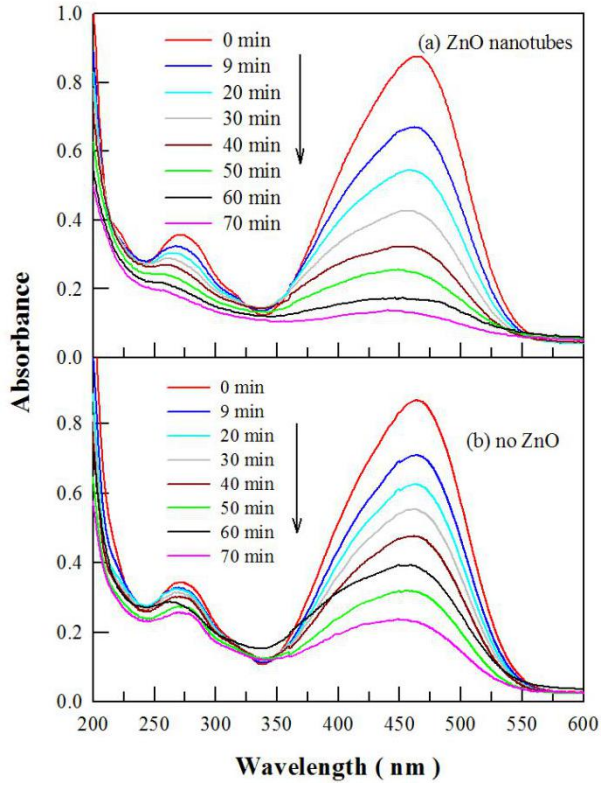

Fig. 5 Evolution of the absorption spectrum of methyl orange solution with the irradiation time of the high-pressure mercury lamp: (a) in the presence of vertically aligned ZnO nanotubes; (b) in the absence of the ZnO nanotubes.

3.3 Photocatalytic activity of ZnO nanotubes

Fig. 5 displays the evolution of absorption spectrum of methyl orange solution with the irradiation time of the high-pressure mercury lamp (a) in the presence of vertically aligned ZnO nanotubes and (b) in the absence of vertically aligned ZnO nanotubes (b). A comparison of the data in Fig. 5 shows clearly that both the photolysis and the photocatalytic degradation happen to the methyl orange in water when illuminated by the high-pressure mercury lamp. It is established that the photocatalytic degradation of organics in solution is initiated by the photoexcitation of the ZnO, followed by the formation of an electron-hole pair on the surface of the ZnO catalyst. Ultimately, the hydroxyl radicals are generated in both the reactions. These hydroxyl radicals are very oxidative in nature and non selective with redox potential of E0 = 2.8 V to oxidize organic compounds into fragments [8]. In our case, the hollow structure of ZnO nanotubes and the immobilization of the ZnO nanotubes can therefore provide a large surface area for the degradation of contaminant molecules. However, the data in Fig. 5 demonstrate that the ZnO nanotubes exhibit only limited photocatalytic activity with respect to the dominant photolysis. Mass transfer limitations become a dominant factor when immobilized photocatalyst film is used, which usually lead to a lower overall degradation rate compared to the suspended catalyst systems. The very low catalyst loading (75 mg/L) is another factor to be responsible for the limited photocatalytic activity of the vertically aligned ZnO nanotubes.

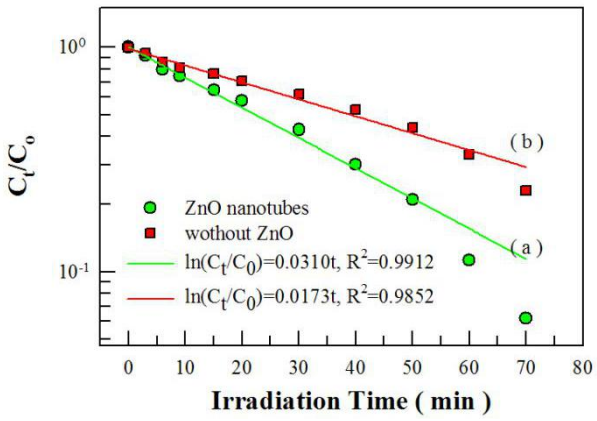

Fig. 6 Semi-log plots of Ct/Co as a function of irradiation time of the high-pressure mercury lamp: (a) in the presence of ZnO nanotubes (circles); (b) in the absence of ZnO nanotubes (squares).

The Langmuir-Hinshelwood kinetic model is widely used to describe the kinetics of photodegradation of many organic compounds. This model can be simplified to a pseudo first-order expression when the concentration of reagent being reacted is very low

$$C_t = C_0 \exp(-kt) \qquad (2)$$

where C_o is the initial concentration of dye, C_t is the concentration of dye at instant t, and k is the pseudo first-order kinetic rate constant [4,8]. The photocatalytic kinetic rate constant for the methyl orange degradation can be determined using Eq. (2). Fig. 6 shows the semi-logarithmic plots of C_t/C_o of the methyl orange solution versus the irradiation time of the high-pressure

mercury lamp (a) in the presence of the vertically aligned ZnO nanotubes (circles) and (b) in the absence of the vertically aligned ZnO nanotubes (squares). The solid lines in Fig. 6 represent the curve fitting of the data with Eq. (2). The semi-log plots of dye concentration versus time were linear, suggesting the first order reactions for both the photolysis and the overall photodegradation. Under the condition of catalyst loading of 75 mg/L, the first-order kinetic rate constant of the photolysis was derived to be 1.73×10^{-2} min^{-1} whilst the first-order kinetic rate constant of the overall photodegradation was 3.10×10^{-2} min^{-1}. As a result, the first-order photocatalytic rate constant of the vertically aligned ZnO nanotubes was derived to be 2.6×10^{-3} min^{-1} by deducing photolysis from the global photodegradation.

3.3 Effect of catalyst loading on the photocatalytic activity of ZnO nanotubes

It was reported that the photocatalytic activity of a catalyst heavily depends on the catalyst loading [27-30]. The effect of the catalyst loading on the photocatalytic activity of the vertically aligned ZnO nanotubes is depicted in Fig. 7. As shown in Fig. 7, the first-order photocatalytic rate constant of the vertically aligned ZnO nanotubes increases monotonically from 0.0026 to 0.023 min-1 as the catalyst loading increases from 75 to 900 mg/L. As the catalyst loading is increased, the number of active sites on the photocatalyst surface will increase too, which in turn generates more hydroxyl and superoxide radicals in the solution. That is the reason why the first-order photocatalytic rate constant of the vertically aligned ZnO nanotubes increases linearly with the catalyst loading. As a contrast to the ZnO catalysts in the form of nanoparticles, neither aggregation of ZnO nanotubes nor loss in the opacity of the solution was observed when more and more immobilized ZnO nanotubes were put into the reactor.

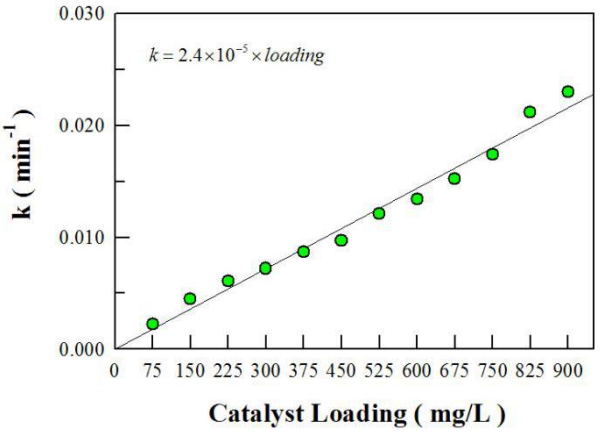

Fig. 7 Catalyst loading dependent photocatalytic rate constant of the vertically aligned ZnO nanotubes.

These vertically aligned ZnO nanotubes on glass substrate exhibit good recyclability. Without any filtration or precipitation after each cycle of photocatalysis, the ZnO nanotubes on glass substrate can be recovered easily and efficiently by simply pulling the glass substrates out of the solution, rinsing with deionized water and drying in air. Our repeated tests showed that the loss in the photocatalytic activity of the vertically aligned ZnO nanotubes was negligible after 20 catalytic cycles. The excellent recyclability demonstrates that the vertically aligned ZnO nanotubes in the form of immobilized films can be utilized as filter-free and cost-effective photocatalyst for large-scale water treatment.

4. Conclusions

Vertically aligned ZnO nanotubes with the average length of 1 μ m, outer diameter of around 500 nm and wall thickness of about 30 nm were grown on glass substrates by hydrothermal growth and subsequent selective etching of ZnO nanorods solutions. The SEM and XRD characterizations have shown that the c-axis of the wurtzite ZnO nanotubes is aligned perpendicularly to the glass substrates. It is found that both photolysis and photocatalytic degradation happen to the methyl orange under the illumination of a 100 W high-pressure mercury lamp. The kinetics of photocatalytic degradation is highlighted, and the first-order photocatalytic constant of the methyl orange is determined. Under the illumination of 100 W high-pressure mercury lamp, the first-order photocatalytic constant of methyl orange has been found to increase linearly from 2.6×10-3 to 2.3 ×10-2 min-1 as the catalyst loading increases from 75 to 900 mg/L. With the advantage of excellent recyclability, ZnO nanotubes in the form of immobilized films can be utilized as filter-free and cost-effective photocatalyst for large-scale water treatment.

Acknowledgment

This work was financially supported by Natural Science Foundation of China under the Grant No 11574036 and 1604028.

References

[1] A. Mclaren, T. Valdes-Solis, G. Li, S.C. Tsang, Shape and size effects of ZnO nanocrystals on photocatalytic activity. *J. Am. Chem. Soc.* 131 (2009) 12540－12541.

[2] X.Y. Zhang, J.Q. Qin, Y.N. Xue, P.F. Yu, B. Zhang, L.M. Wang, R.P. Liu, Effect of aspect ratio and surface defects on the photocatalytic activity of ZnO nanorods. *Sci. Rep.* 4 (2014) 4596.

[3] S. Baruah, M. Jaisai, R. Imani, M.M Nazhad, J. Dutta, Photocatalytic paper using zinc oxide nanorods. *Sci. Technol. Adv. Mater.* 11 (2010) 055002

[4] D. Chu, Y. Masuda, T. Ohji, K. Kato, Formation and photocatalytic application of ZnO nanotubes using aqueous solution. *Langmuir* 26 (2010) 2811－2815.

[5] F. Xu, J. Chen, L. Guo, S. Lei, Y. Ni, In situ electrochemically etching-derived ZnO nanotube arrays for highly efficient and facilely recyclable photocatalyst. *Appl. Surf. Sci.* 258 (2012) 8160－8165.

[6] Y.M. Huang, Q.L. Ma, B.G. Zhai, Core-shell Zn/ZnO structures with improved photocatalytic properties synthesized by aqueous solution method. *Funct. Mater. Lett.* 6 (2013) 1350058

[7] Q.L. Ma, R. Xiong, B.G. Zhai, Y.M. Huang, Core-shelled Zn/ZnO microspheres synthesized by ultrasonic irradiation for photocatalytic applications. *Micro Nano Lett.* 8 (2013) 491－495.

[8] Q.L. Ma, R. Xiong, B.G. Zhai, Y.M. Huang, Ultrasonic synthesis of fern - like ZnO nanoleaves and their enhanced photocatalytic activity. *Appl. Surf. Sci.* 324 (2015) 842－848.

[9] Y.M. Huang, B.G. Zhai, F.F. Zhou, Effects of photo-irradiation on the optical properties and electronic structures of an azo-containing bent-core liquid crystal. *Mol. Cryst. Liq. Cryst.* 510 (2009) 34－42.

[10] H.C. Yatmaz, A. Akyol, M. Bayramoglu, Kinetics of the photocatalytic decolorization of an azo reactive dye in aqueous ZnO suspensions. *Ind. Eng. Chem. Res.* 43 (2004) 6035－6039.

[11] U.G. Akpan, B.H. Hameed, Parameters affecting the photocatalytic degradation of dyes using TiO2-based photocatalysts: A review. *J. Hazard. Mater.* 170 (2009) 520－529.

[12] T.K. Tseng, Y.S. Lin, Y.J. Chen, H. Chu, A review of photocatalysts prepared by sol-gel method for VOCs removal, *Int. J. Mol. Sci*. 2010, 11, 2336－2361.

[13] K. Hashimoto, H. Irie, A. Fujishima, TiO2 photocatalysis: a historical overview and future prospects. *Jpn. J. Appl. Phys.* 44 (2015) 8269－8285.

[14] L. Yang, Q.L. Ma, Y.G. Cai, Y.M. Huang, Enhanced photovoltaic performance of dye sensitized solar cells using one dimensional ZnO nanorod decorated porous TiO_2 electrode. *Appl. Surf. Sci.* 292 (2014) 297－300.

[15] L. Yang, B.G. Zhai, Q.L. Ma, Y.M. Huang, Effect of ZnO decoration on the photovoltaic performance of TiO_2 based dye sensitized solar cells. *J. Alloy. Compd.* 605 (2014) 109－112.

[16] Q.L. Ma, Y.M. Huang, Improved Photovoltaic performance of dye sensitized solar cell by decorating TiO_2 photoanode with Li-doped ZnO nanorods. *Mater. Lett.* 148 (2015) 171－173.

[17] L. Roza, M.Y.A. Rahman, A.A. Umar, M.M. Salleh, Direct growth of oriented ZnO nanotubes by self-selective etching at lower temperature for photo-electrochemical (PEC) solar cell application. *J. Alloy. Compd.* 618 (2015) 153－158.

[18] Y.M. Huang, Q.L. Ma, B.G. Zhai, Controlled morphology of ZnO nanostructures by adjusting the zinc foil heating temperature in an air-filled box furnace. *Mater. Chem. Phys.* 147 (2014) 788－795.

[19] J. Yang, Y. Lin, Y. Meng, Y. Liu, A two-step route to synthesize highly oriented ZnO nanotube arrays. *Ceram. Int.* 38 (2012) 4555－4559.

[20] X. Ma, M. Gao, J. Zheng, H. Xu, G. Li, Conversion of large-scale oriented ZnO rod array into nanotube array under hydrothermal etching condition via one-step synthesis approach. *Physica E* 42 (2010) 2237－2241.

[21] Y.M. Huang, Q.L. Ma, B.G. Zhai, Wavelength tunable photoluminescence of ZnO/porous Si nanocomposites. *J. Lumin.* 138 (2013) 157－163.

[22] O. Lupan, V.M. Guérin, I.M. Tiginyanu, V.V. Ursaki, L. Chow, H. Heinrich, T. Pauporté, Well-aligned arrays of vertically oriented ZnO nanowires electrodeposited on ITO-coated glass and their integration in dye sensitized solar cells. *J. Photoch. Photobio. A* 211 (2010) 65－73.

[23] Y.M. Huang, Q.L. Ma, B.G. Zhai, Wavelength tunable photoluminescence of ZnO/porous Si nanocomposites. *J. Lumin*. 138 (2013) 157－163.

[24] M.D. McCluskey, S.J. Jokela, Defects in ZnO. *J. Appl. Phys.* 106 (2009) 071101.

[25] Y.M. Huang, Q.L. Ma, B.G. Zhai, A simple method to grow one-dimensional ZnO nanostructures in air. *Mater. Lett.* 93 (2013) 266－268.

[26] B.G. Zhai, Y.M. Huang, Origin of thermal‐annealing induced orange emissions from solution‐grown ZnO nanocrystals. *Mater. Res. Innov.* 19 (2015) 19 s45－s50.

[27] N. Daneshvar, D. Salari, A. R. Khataee, Photocatalytic degradation of azo dye acid red 14 in water on ZnO as an alternative catalyst to TiO_2. *J. Photoch. Photobio. A* 162 (2004) 317－322.

[28] M.A. Behnajady, N. Modirshahla, R. Hamzavi, Kinetic study on photocatalytic degradation of C.I. Acid Yellow 23 by ZnO photocatalyst. *J. Hazard. Mater.* 133 (2006) 226－232.

[29] C.C. Chen, Degradation pathways of ethyl violet by photocatalytic reaction with ZnO dispersions. *J. Mol. Catal. A-Chem*. 264 (2007) 82-92.

[30] A. Akyol, H.C. Yatmaz, M. Bayramoglu, Photocatalytic decolorization of remazol red RR in aqueous ZnO suspensions. *Appl. Catal. B-Environ*. 54 (2004) 19－24.